Impact of Mesoporous Titania-Perovskite Interface on the Performance of Hybrid Organic-Inorganic Perovskite Solar Cells

Mojtaba Abdi-Jalebi[‡], M. Ibrahim Dar*[§], Aditya Sadhanala[‡], Satyaprasad P. Senanayak[‡], Fabrizio Giordano[§], Shaik Mohammed Zakeeruddin[§], Michael Grätzel[§], Richard H. Friend*[‡]

[‡] Cavendish Laboratory, JJ Thomson Avenue, Cambridge CB3 0HE, United Kingdom.

[§] Laboratory of Photonics and Interfaces, Swiss Federal Institute of Technology (EPFL), Station 6, Lausanne, CH 1015, Switzerland.

* ma571@cam.ac.uk, ibrahim.dar@epfl.ch, rhf10@cam.ac.uk,

We report on the optimization of the interfacial properties of titania in mesoscopic $CH_3NH_3PbI_3$ solar cells. Modification of the mesoporous-TiO_2 film by $TiCl_4$ treatment substantially reduced the surface traps, as evident from sharpness of the absorption edge with a significant reduction in Urbach energy (320 meV to 140 meV) determined from photothermal deflection spectroscopy and lead to an order of magnitude enhancement in the bulk electron mobility and corresponding decrease in the transport activation energy (170 meV to 90 meV) within a device. After optimization of the photoanode-perovskite interface using various sizes of TiO_2 nanoparticles, the best photovoltaic efficiency of 16.3% was achieved with the mesoporous-TiO_2 composed of 36 nm sized nanoparticles. The improvement in device performance can be attributed to the enhanced charge collection efficiency that is driven by improved charge transport in the mesoporous TiO_2 layer. Also, the decreased recombination at the TiO_2-perovskite interface and better perovskite coverage play an important role.

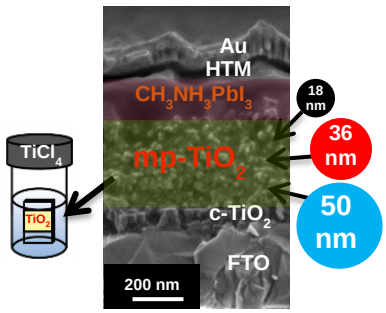

Keywords: Perovskite solar cell; $TiCl_4$ post treatment; mp-TiO_2; energetic disorder; nanoparticle size; interface

Recent developments in using hybrid organic-inorganic perovskites as light absorbers have raised the power conversion efficiency (PCE) of solid state mesoscopic solar cells above 20% level[1–3]. Such an impressive efficiency was achieved due to desired properties including a high absorption coefficient, an ideal/tuneable band-gap and long carrier diffusion lengths as well as photon recycling capability of hybrid organic-inorganic perovskite materials[4–10]. A typical mesoscopic perovskite solar cell (PSC) contains a blocking TiO_2 (bl-TiO_2) layer, mesoporous TiO_2 (mp-TiO_2), hybrid organic-inorganic perovskite sensitizers, hole transporting material (HTM) and counter electrode (e.g. Au) as the key components. The mp-TiO_2 layer in a typical dye-sensitized solar cell (DSSC) plays three major roles; provides a scaffold to increase the surface area of the absorber layer, act as a hole blocker, and transports photogenerated electron from the sensitized surface to the front contact[11]. Therefore, the active surface area which has a direct link with particle size of mesoporous material is a key parameter in DSSC[12]. However, Lee et al. have shown that hybrid organic-inorganic perovskite absorber can transport photogenerated electron to the conductive substrate itself[13]. On the other hand, it is reported that employing the mesoporous TiO_2 layer substantially reduces the hysteresis behaviour of PSC[14]. In addition, it is widely recognized that the interface between the absorber layer and the carrier transport layers, as well as the inherent carrier transporting properties of the layers are also important. An ideal carrier transport material is expected to possess a suitable energy level, high conductivity, and low surface recombination rate. Several materials have been investigated as electron transport layers (ETL) such as TiO_2, ZnO and phenyl-C_{61}-butyric acid methyl ester (PCBM)[15–18]. Among all of them, TiO_2 arguably is the most commonly used ETL has delivered the best photovoltaic

performance in PSC thus far[19]. To improve the performance of mesoscopic solar cells, further investigation is needed to engineer the mp-TiO_2-perovskite interface[20,21].

In this study, we explored the effect of $TiCl_4$ post-treatment of mp-TiO_2 on the optical behaviour and the level of electronic disorder using space charge limited current (SCLC) technique and photothermal deflection absorption spectroscopy (PDS) and correlated our findings with the photovoltaic behaviour of the fabricated PSC. We further extended the study by investigating the effect of the titania nanoparticle size on the charge transport, recombination properties, optical behaviour and the photovoltaic performance of PSC. For a comparative analysis, we synthesized two alkaline TiO_2 pastes (NP36 and NP50) and compared them with commercial 18NRT dyesol TiO_2 nanoparticles. Finally, based on our new findings, we suggest the main criteria for the mp-TiO_2 in acting as an ideal electron transport layer for achieving the high efficiency in PSCs.

We used a typical structure of PSC which consists of spray coated titania compact layer on fluorine-doped tin oxide (FTO) coated glass, spin-coated mp-TiO_2, sequential two-step spin-coated $CH_3NH_3PbI_3$ perovskite, spiro OMETAD as a hole transport layer and back contact of thermally evaporated gold layer. It is notable a capping layer of perovskite is formed on top of the mp-TiO_2 layer (Figure S1). We optimized the thickness of mp-TiO_2 which is a key parameter to achieve high PCE (see details in supporting information).

In DSSC, $TiCl_4$-treatment of mp-TiO_2 electrode prior to the device fabrication improves the performance of the photovoltaic devices[22], because of several phenomena, such as an increase in the electron injection rate, a retardation of the electron–hole recombination and/or an increase in the dye loading. However, the exact mechanism of the improvement is not clearly understood[23].

Herein, we investigated the effect of $TiCl_4$-treatment on the morphology and absorption of 36 nm sized mp-TiO_2 as well as on the device performance (Table 1). SEM images of the pristine and treated mp-TiO_2 showed that a very thin layer of compact titania covered the surface of TiO_2 nanoparticles (Figure 1a, b). Upon $TiCl_4$ treatment, the photovoltaic devices exhibit an increase in the open circuit voltage (V_{oc}) by 50 mV, in addition to the marginal improvement in the short circuit current (J_{sc}) and fill factor (FF) which gets reflected in the overall efficiencies of the PSC (16.1%). It is notable that the coverage and morphology of perovskite capping layer has not altered upon this treatment (Figure S2).

Based on the PDS measurements (Figure 1c), $TiCl_4$ treatment significantly reduced the sub-bandgap absorption and increased the density of states near the titania band-edge that has been shown to improve the mobility in metal oxides and could potentially improve the charge transport within the mp-layer in a solar cell configuration[24,25]. In a PDS spectra, the slope of the absorption at the band edge defines the Urbach energy (E_u), and provides a measure for the degree of energetic disorder of a material[26,27]. The estimated Urbach energy for the pristine and $TiCl_4$ post treated titania, along with the respective fitting errors (Figure S7), are 320 and 140

Table 1. Summary of the photovoltaic parameters extracted from J–V measurements under simulated AM1.5G irradiation and electron mobility along with activation energy and the corresponding errors for devices (batch of 20 devices) based on 300nm thick mp-TiO_2 without (pristine) and with $TiCl_4$ post-treatment.

Type of device	J_{SC} (mA cm^{-2})	V_{OC} (mV)	FF	PCE (%)	μ_e (cm^2/Vs)	E_A^e (meV)
Pristine	21.36±0.3	970±12	0.70±0.02	15.2±0.3	0.002±0.001	170±15
$TiCl_4$ post-treated	22.12±0.1	1020±10	0.71±0.01	16.1±0.2	0.03±0.006	95±9

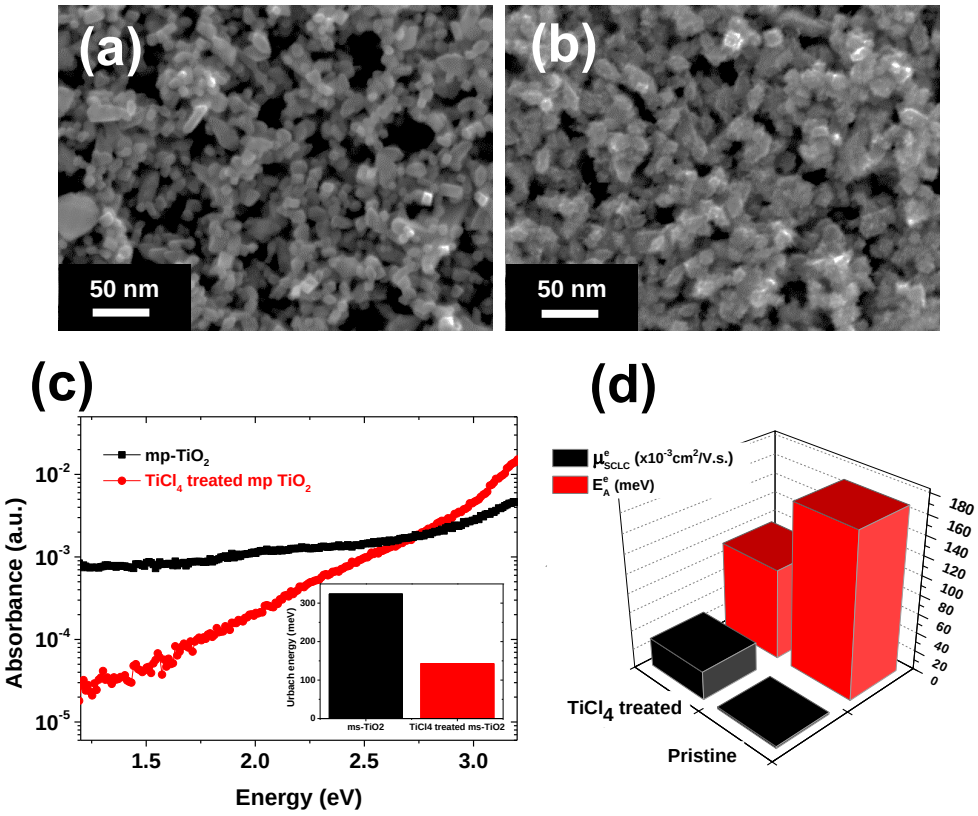

Figure 1. (a) Top view SEM images of pristine mp-TiO_2 film and (b) with $TiCl_4$ post-treatment. (c) The PDS absorbance spectra of mp-TiO_2 films, pristine and $TiCl_4$ post-treated. The inset shows the corresponding Urbach energies. (d) Effect of $TiCl_4$ treatment on Electron mobility and activation energy in the fabricated device.

meV, respectively (inset of Figure 1c).

Furthermore, a direct estimation of the disorder is obtained from a measure of the activation energy (E_A^e) acquired from the temperature-dependent bulk transport measurements. Based on this measurement on electron-only devices FTO/TiO_2 (treated or untreated)/Perovskite/Al, we estimated the electron mobility (μ_{SCL}^e) ~ 0.002 $cm^2.V^{-1}.s^{-1}$ for pristine devices which increases to around 0.03 $cm^2.V^{-1}.s^{-1}$ upon the treatment (Table1). Correspondingly, the E_A^e decreases from 170 meV to 95 meV for $TiCl_4$-treated mp-TiO_2 based PSC (Figure 1d). This enhancement in the electron mobility in addition to passivation of trap states at the perovskite–titania interface which considerably minimizes the recombination of the charge carriers and enhances

charge transport can then be correlated to the enhanced V_{oc}, J_{sc} and the overall PCE of devices[28].

To further understand the role of the titania interlayer on the photovoltaic performance, we investigated three different particle sizes of mp-TiO_2 using two synthesised titania with 36 nm (NP36) and 50 nm (NP50) sized nanoparticles based on the reported procedure[29] and the commercial 18NRT dyesol titania paste. The aspects of these titania pastes and structural characterization of the deposited films are provided in the supporting information.

PDS of different sized mp-TiO_2 films shows that the sub-bandgap absorption is lower for both NP36 and NP50 compare to 18NRT and the estimated E_u is the lowest for NP36 (140 meV) representative of the lowest level of electronic disorder (Figure 2a). To extract further information on the light-induced charge injection/separation, we performed time-resolved photoluminescence (PL) decay measurements on the $CH_3NH_3PbI_3$ deposited on different mp-TiO_2 films (Figure 2b). Using standard biexponential fits (Figure S13), the PL decay of the infiltrated perovskite in 18NRT, NP36 and NP50 films exhibits a time-constant of τ_1= 1.06 ns, 4.49 ns and 6.76 ns, respectively. It is evident that the temporal decay of PL intensity become faster, as the nanoparticle size of the TiO_2 reduces.

The PL decay of the aforementioned films arises from quenching of the PL intensity (Figure S14) because of the following two reasons; first, radiative relaxation of excited electrons back to the ground state of perovskite, second, electron injection from the conduction band of perovskite into the conduction band of titania. Because the radiative relaxation back to the ground state of perovskite occurs at a certain inherent rate that corresponds to the PL decay rate of the bare $CH_3NH_3PbI_3$ shown in Figure 2b, the acceleration of the PL decay rate with the reduction of the titania

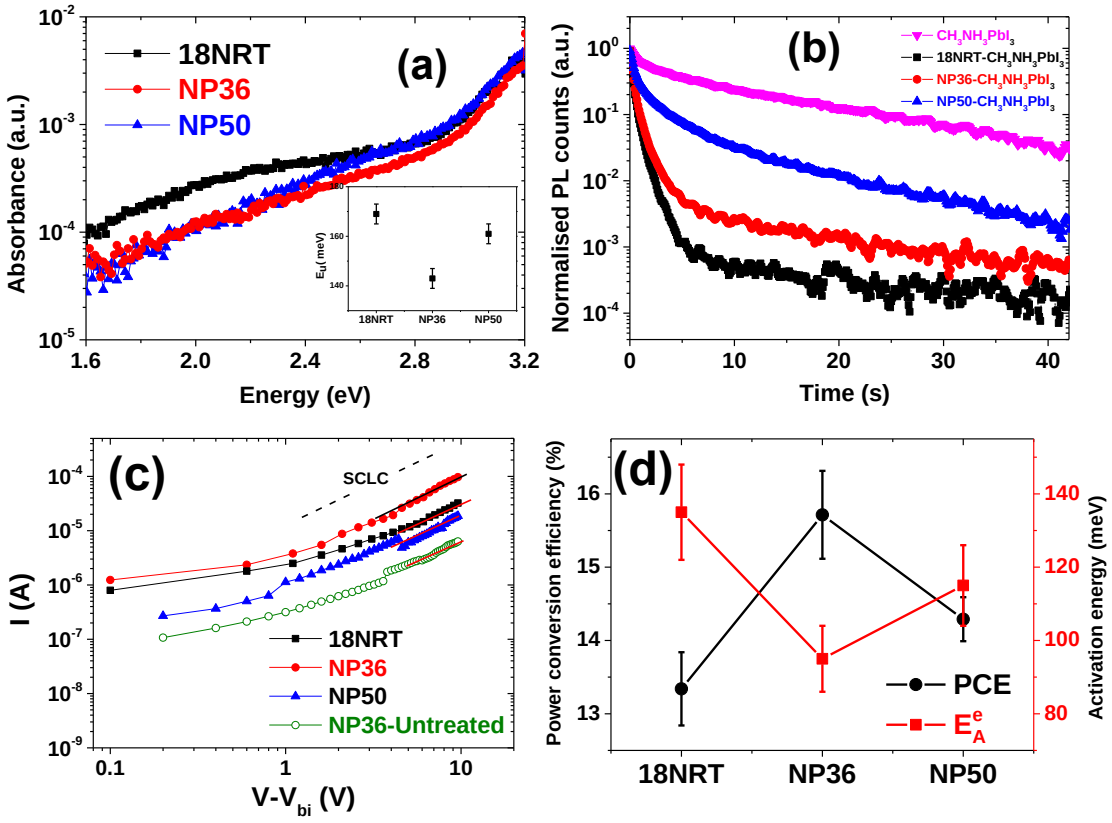

Figure 2. (a) The PDS absorption spectra of different mp-TiO_2 films. The inset shows the corresponding Urbach energies for all the titania films. The error bar is defined by the s.d in fitting the Urbach tail (Figure S12). (b) Fluorescence decay kinetics measured at 780 nm upon excitation at 407 nm with fluence of 0.7 nJ.cm^{-2} for perovskite films deposited on different mp-TiO_2 layers. (c) *I–V* characteristics of electron only devices (FTO/TiO_2/Perovskite/AL), utilized for estimating the SCLC electron mobility. (d) The trends in the PCE and E_A^e for PSC based on different sized mp-titania layers.

nanoparticle size in the TiO_2/$CH_3NH_3PbI_3$ films indicates more efficient injection of electrons from the perovskite to TiO_2. Therefore, we can infer that, as the size of TiO_2 nanoparticles become smaller, the electron injection from perovskite to TiO_2 becomes more efficient.

It is well established that not only the precursor compositions of perovskite[30,31] but also the substrate can influence the growth and formation of perovskite films[32,33].

Top-view SEM images of perovskite capping layer on mp-TiO_2 shows that NP36 has the best coverage as the titania layer is fully covered by perovskite crystals while in both 18NRT and NP50, we observe some pinholes in between the perovskite grains (Figure S15).

In order to investigate the effect of modification of TiO_2 layer on the electron transport behavior, we fabricated electron only (FTO/TiO_2/Perovskite/Al) devices for SCLC measurement (see details in supporting information)[34]. Remarkably, our transport measurements indicate a clear trend where the μ_{SCL}^{e} and E_A^e were altered upon modification of mp-TiO_2 (Table 2, Figure 2c, d). Electron mobility as high as (μ_{SCL}^{e}) 0.03 $cm^2.V^{-1}.s^{-1}$ and the lowest activation energy of 95 meV was obtained for NP36 based devices (Figure S16). Therefore, the disorder in the perovskite is strongly affected by the layer on which it is deposited[35]. The observed enhancement in the μ_{SCL}^{e} and the decrease in E_A^e is expected to improve the J_{sc} and decrease the recombination which could enhance the V_{oc} resulting in an overall improvement in the PCE.

Hence, as a next step, photoanodes based on different sized mp-TiO_2 were used to explore particle size effect on the photovoltaic performance of PSC (Table 2 and

Table 2. Summary of the photovoltaic parameters derived from J-V measurements and charge mobilities along with activation energy for the perovskite solar cells based on different sized mp-TiO_2 (showing the best performance).

Type of device	J_{SC} (mA cm^{-2})	V_{OC} (mV)	FF	PCE (%)	μ_e ($cm^2.V^{-1}.s^{-1}$)	E_A^e (meV)
18NRT	21.32	965	0.673	13.8	0.01± 0.008	135± 13
NP36	22.23	1029	0.709	16.3	0.03±0.005	95± 9
NP50	21.63	948	0.711	14.6	0.008±0.003	115±11

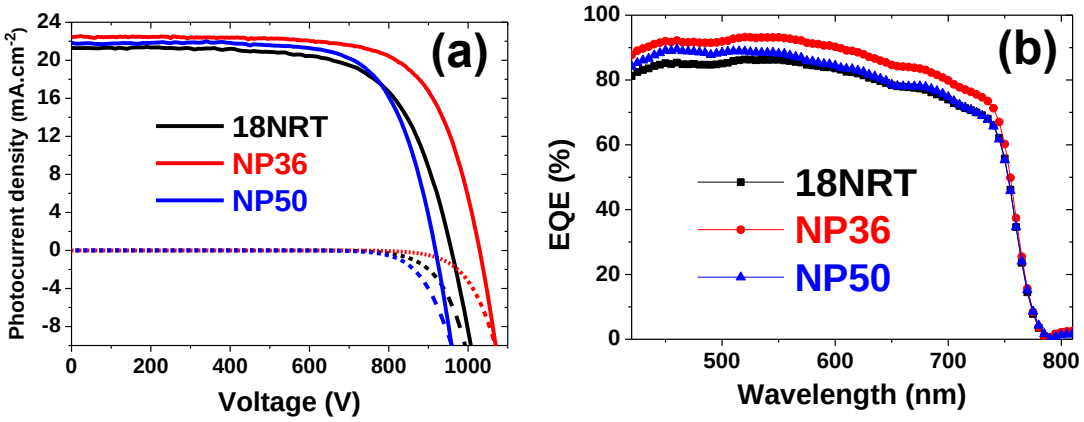

Figure 3. (a) Current-voltage characteristics measured under standard 1 sun conditions (AM 1.5 G, 100 mW.cm^{-2}) (solid lines) and dark conditions (dashed lines) (b) External quantum efficiency (EQE) spectra as a function of the wavelength of monochromatic light for the perovskite solar cells obtained from different mp-TiO_2 nanoparticles.

Figure 3a). The statistics of the photovoltaic parameters follow the same trend as the best performing devices (Figure S18). As the diameter of the particles increases from 18 nm to 36 nm, the average J_{sc} rises from 21.1 mA.cm^{-2} to 22.3 mA.cm^{-2}. This trend in J_{sc} can be attributed to the narrow tunnels in the 18 nm TiO_2 mesoscopic framework in which the perovskite cannot infiltrate till the bottom of the TiO_2 layer easily. However, in the NP36, the improved pore filling caused by a larger pore size leads to an enhancement of the J_{sc}. This is consistent with UV-Vis absorption spectra, which shows a higher absorption above the band edge for the perovskite deposited on NP36 compare to 18NRT (Figure S19). Further increase of the TiO_2 particle size to 50 nm causes a slight decline in the photocurrent density which may be ascribed to the pronounced scattering properties of larger titania nanoparticles (Figure S8) as well as the reduction of the porosity which minimizes the amount of perovskite in the mesoscopic TiO_2 framework. The enhancement in current densities of PSC based on

different size of mp-TiO_2 nanoparticles are supported by the improvement in the external quantum efficiency (EQE) spectra shown in Figure 3b.

As shown in Table 2, the FF increases from 0.67 to 0.71 when the size of TiO_2 nanoparticle's increases from 18 nm to 36 nm and remains the same for NP50, which might be attributed to the reduction in the electron transport resistance of the TiO_2 mesoscopic structure and better filling of the perovskite. In addition, the average value of V_{oc} climbed from 970 mV to 1029 mV by changing the TiO_2 average particle size from 18 nm to 36 nm. Our observations indicate that NP36 exhibit the optimum pore size for efficient infiltration of the perovskite into the mp-TiO_2 (Figure S15), the highest electron mobility and the lowest disorder in the interface with perovskite which result in the enhancement of V_{oc}, J_{sc} and a maximum PCE of 16.3%.

Based on the J-V characteristic of the devices under dark, the dark current onset begins at around 600 mV for the NP50 while it shifts to ~650 and ~750 mV for 18NRT and NP36, respectively (Figure 3a). On forward biasing, the recombination of the photogenerated electrons at the interfaces between FTO or TiO_2 and HTM is a potential source of dark current. Here, the recombination at the TiO_2-HTM interface for NP50 might be due to the weak coverage of the pores with perovskite that dominates and leads to lower V_{oc} while the effect of recombination from the FTO-HTM interface is negligible due to the complete coverage of FTO by a compact TiO_2 layer.

To study the charge transfer and recombination processes in a PSC based on various sized mp-TiO_2, we performed intensity modulated photovoltage spectroscopy (IMVS) shown in Figure 4a. The electron recombination time constant (τ_r) as a function of titania particle size, which is calculated using $\tau_r = 1/2\pi f_r$, where f_r is the characteristic frequency minimum of an IMVS curve. The increased τ_r from 18NRT to NP36

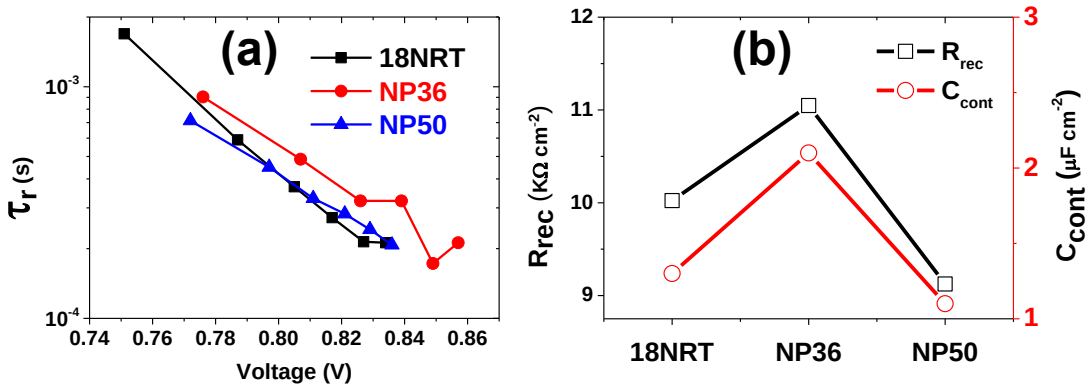

Figure 4. (a) Comparison of τ_r for the PSC based on different sized mp-titania layers. (b) The trends in the R_{rec} and C_{cont} for PSCs based on various mp-TiO_2 layers.

suggests a reduction of the electron recombination process in the PSC. This could be attributed to two factors; firstly, the lowest electronic disorder at the TiO_2-perovskite interface, secondly, the improved blocking effect of perovskite overlayer for NP36, which showed the best perovskite coverage, and potentially helps in reducing the electron-hole recombination between TiO_2 and HTM. However, when the size of TiO_2 nanoparticles is further increased (NP50), higher disorder in the titania layer increases the number of trap sites in the device structure eventually leading to a possibility of electron-hole recombination and hence τ_r decreases [36].

To further understand the transport mechanism, we utilize electrochemical impedance spectroscopy (EIS) on PSC fabricated with different mp-TiO_2 layers. The EIS measurement was performed on the complete photovoltaic devices operating under illumination and open circuit conditions (Figure S21). The EIS spectra were fitted with an appropriate equivalent circuit to estimate parameters related to the charge recombination and polarization relaxation of the perovskite layers (see details in supporting information). Based on the fitting of the equivalent circuit to the EIS data, we obtain the recombination resistance to be maximum for NP36 which is consistent

with the trend of higher J_{sc} magnitude (Figure 4b). Correspondingly, the large area in the EIS of the NP50 can be correlated to higher series resistance which is in agreement with the lower J_{sc} magnitude. Differences in the trend of V_{oc}, J_{sc} and FF of the PSC with the parameters of the EIS spectra arises due to the preliminary level of the equivalent circuit utilized for the fitting.

In general, the observation of higher value of J_{sc} in a photovoltaic device can be related to a range of factors. This includes enhanced transport in the active layer which supports lower recombination and enhanced charge collection at the adjacent contacts. Since we compare photovoltaic devices with identical active layer fabricated under the same conditions, the differences originating from the charge transport in the active layer can be completely ignored. Hence, the variation in the R_{rec} can be attributed to the collection efficiency of the interface. Similarly, the enhancement of the C_{cont} for a particular photovoltaic cell based on NP36 directly correlates with the enhancement of the V_{oc}.

In summary, we have systematically studied the different parameters to explore the influence of TiO_2-perovskite interface for mesoscopic perovskite solar cells. We showed that the $TiCl_4$ post treatment of the mp-TiO_2 film prior to device fabrication passivate the titania surfaces, increases the density of states and reduces the disorder level which significantly enhances the open circuit voltage (~ 50mV) and the device performance. Furthermore, different sized TiO_2 nanoparticles were applied as electron acceptors in the mesoscopic PSC. The particle size effect of TiO_2 nanoparticles on the photovoltaic performance of PSC was investigated which not only influences the contact between the perovskite crystal-TiO_2, but also significantly affects the charge transfer kinetics at the TiO_2-perovskite interface and the overall disorder of the perovskite layer for charge transport. We observe that the particle size of 36 nm is

optimum for obtaining the best performance solar cells with consistent and reproducible PSC of 16.3%. Based on transport, spectroscopic and photovoltaic measurements, we conclude that the mp-TiO_2 interlayer should have the least energetic disorder, optimum particle and pore size in order to enhance the homogeneous growth of perovskite over-layer and optimum charge transport properties to realise high efficiency in mesoscopic perovskite solar cells.

AUTHOR INFORMATION

Corresponding Author

*E-mail: ma571@cam.ac.uk, ibrahim.dar@epfl.ch, rhf10@cam.ac.uk

Notes

The authors declare no competing financial interest.

ACKNOWLEDGEMENTS

M.A.J. thanks Nava Technology Limited for a PhD scholarship. A.S. gratefully acknowledges financial support from the Indo-UK APEX project. S.P.S. acknowledges Royal Society London for the Newton Fellowship. R.H.F, M.A.J., and A.S. would like to acknowledge the support from EPSRC. M.I.D., S.M.Z. and M.G. thank the King Abdulaziz City for Science and Technology (KACST) and Swiss National Science Foundation (SNSF) for financial support.

ASSOCIATED CONTENT

Supporting Information

Experimental procedures, cross sectional and top view SEM images, optimization of the thickness of mp-TiO_2, the aspects and structural characterization of different mp-TiO_2 pastes and films, data fitting of Urbach energy for PDS measurement, fitting curves for fluorescence decay kinetics measurement, details of SCLC and EIS characterisations and statistics for photovoltaic measurements are provided.

REFERENCES

(1) Yang, W. S.; Noh, J. H.; Jeon, N. J.; Kim, Y. C.; Ryu, S.; Seo, J.; Seok, S. Il. High-Performance Photovoltaic Perovskite Layers Fabricated through Intramolecular Exchange. *Science* **2015**, *348* (6240), 1234–1237.

(2) Yi, C.; Li, X.; Luo, J.; Zakeeruddin, S. M.; Grätzel, M.; McMeekin, D. P.; Sadoughi, G.; Rehman, W.; Eperon, G. E.; Saliba, M.; et al. Perovskite Photovoltaics with Outstanding Performance Produced by Chemical Conversion of Bilayer Mesostructured Lead Halide/TiO2 Films. *Science* **2016**, *351* (6269), 151–155.

(3) Li, X.; Bi, D.; Yi, C.; Decoppet, J.-D.; Luo, J.; Zakeeruddin, S. M.; Hagfeldt, A.; Gratzel, M. A Vacuum Flash-Assisted Solution Process for High-Efficiency Large-Area Perovskite Solar Cells. *Science* **2016**, *353* (6294), 58–62.

(4) Marchioro, A.; Teuscher, J.; Friedrich, D.; Kunst, M.; van de Krol, R.; Moehl, T.; Grätzel, M.; Moser, J.-E. Unravelling the Mechanism of Photoinduced Charge Transfer Processes in Lead Iodide Perovskite Solar Cells. *Nat. Photonics* **2014**, *8* (3), 250–255.

(5) Snaith, H. H. J. Perovskites: The Emergence of a New Era for Low-Cost, High-Efficiency Solar Cells. *J. Phys. Chem. Lett.* **2013**, *4* (21), 3623–3630.

(6) Park, N. N. Organometal Perovskite Light Absorbers toward a 20% Efficiency Low-Cost Solid-State Mesoscopic Solar Cell. *J. Phys. Chem. Lett.* **2013**, *4* (15), 2423–2429.

(7) Xing, G.; Mathews, N.; Sun, S.; Lim, S. S.; Lam, Y. M.; Gratzel, M.; Mhaisalkar, S.; Sum, T. C. Long-Range Balanced Electron- and Hole-Transport Lengths in Organic-Inorganic CH3NH3PbI3. *Science* **2013**, *342* (6156), 344–347.

(8) Stranks, S. D.; Eperon, G. E.; Grancini, G.; Menelaou, C.; Alcocer, M. J. P.; Leijtens, T.; Herz, L. M.; Petrozza, A.; Snaith, H. J. Electron-Hole Diffusion Lengths Exceeding 1 Micrometer in an Organometal Trihalide Perovskite Absorber. *Science* **2013**, *342* (6156), 341–344.

(9) Abdi-Jalebi, M.; Dar, M. I.; Sadhanala, A.; Senanayak, S. P.; Franckevičius, M.; Arora, N.; Hu, Y.; Nazeeruddin, M. K.; Zakeeruddin, S. M.; Grätzel, M.; et al. Impact of Monovalent Cation Halide Additives on the Structural and Optoelectronic Properties of CH 3 NH 3 PbI 3 Perovskite. *Adv. Energy Mater.* **2016**, *6* (10), 1502472.

(10) Pazos-Outon, L. M.; Szumilo, M.; Lamboll, R.; Richter, J. M.; Crespo-Quesada, M.; Abdi-Jalebi, M.; Beeson, H. J.; Vru ini, M.; Alsari, M.; Snaith, H. J.; et al. Photon Recycling in Lead Iodide Perovskite Solar Cells. *Science* **2016**, *351* (6280), 1430–1433.

(11) Chandiran, A. K.; Abdi-Jalebi, M.; Nazeeruddin, M. K.; Grätzel, M. Analysis of Electron Transfer Properties of ZnO and TiO 2 Photoanodes for Dye-Sensitized Solar Cells. *ACS Nano* **2014**, *8* (3), 2261–2268.

(12) Abdi-Jalebi, M.; Mohammadi, M. R.; Fray, D. J. Double-Layer TiO2 Electrodes with Controlled Phase Composition and Morphology for Efficient Light Management in Dye-Sensitized Solar Cells. *J. Clust. Sci.* **2014**, *25* (4),

1029–1045.

(13) Lee, M. M.; Teuscher, J.; Miyasaka, T.; Murakami, T. N.; Snaith, H. J. Efficient Hybrid Solar Cells Based on Meso-Superstructured Organometal Halide Perovskites. *Science* **2012**, *338* (6107), 643–647.

(14) Kim, H.-S.; Park, N.-G. Parameters Affecting I – V Hysteresis of CH 3 NH 3 PbI 3 Perovskite Solar Cells: Effects of Perovskite Crystal Size and Mesoporous TiO 2 Layer. *J. Phys. Chem. Lett.* **2014**, *5* (17), 2927–2934.

(15) Chiang, C.-H.; Wu, C.-G. Bulk Heterojunction perovskite–PCBM Solar Cells with High Fill Factor. *Nat. Photonics* **2016**, *10* (3), 196–200.

(16) You, J.; Meng, L.; Song, T.-B.; Guo, T.-F.; Yang, Y. (Michael); Chang, W.-H.; Hong, Z.; Chen, H.; Zhou, H.; Chen, Q.; et al. Improved Air Stability of Perovskite Solar Cells via Solution-Processed Metal Oxide Transport Layers. *Nat. Nanotechnol.* **2015**, *11* (1), 75–81.

(17) Chandiran, A. K.; Abdi-Jalebi, M.; Yella, A.; Dar, M. I.; Yi, C.; Shivashankar, S. A.; Nazeeruddin, M. K.; Grätzel, M. Quantum-Confined ZnO Nanoshell Photoanodes for Mesoscopic Solar Cells. *Nano Lett.* **2014**, *14* (3), 1190–1195.

(18) Abdi-jalebi, M.; Chandiran, A. K.; Nazeeruddin, M. K.; Grätzel, M. Low Temperature Dye-Sensitized Solar Cells Based on Conformal Thin Zinc Oxide Overlayer on Mesoporous Insulating Template by Atomic Layer Deposition. *Sci. Iran. F* **2014**, *21* (6), 2479–2484.

(19) Bi, D.; Tress, W.; Dar, M. I.; Gao, P.; Luo, J.; Renevier, C.; Schenk, K.; Abate, A.; Giordano, F.; Correa Baena, J.-P.; et al. Efficient Luminescent Solar Cells Based on Tailored Mixed-Cation Perovskites. *Sci. Adv.* **2016**, *2* (1), e1501170–e1501170.

(20) Giordano, F.; Abate, A.; Pablo, J.; Baena, C.; Saliba, M.; Matsui, T.; Im, S. H.; Zakeeruddin, S. M.; Nazeeruddin, M. K.; Hagfeldt, A.; et al. Enhanced Electronic Properties in Mesoporous TiO2 via Lithium Doping for High-Efficiency Perovskite Solar Cells. *Nat. Commun.* **2016**, *7*, 1–6.

(21) Massihi, N.; Mohammadi, M. R.; Bakhshayesh, a. M.; Abdi-Jalebi, M. Controlling Electron Injection and Electron Transport of Dye-Sensitized Solar Cells Aided by Incorporating CNTs into a Cr-Doped TiO2 Photoanode. *Electrochim. Acta* **2013**, *111*, 921–929.

(22) Lee, S. W.; Ahn, K. S.; Zhu, K.; Neale, N. R.; Frank, a J. Effects of TiCl4 Treatment of Nanoporous TiO2 Films on Morphology, Light Harvesting, and Charge-Carrier Dynamics in Dye-Sensitized Solar Cells. *J. Phys. Chem. C* **2012**, *116*, 21285–21290.

(23) Choi, H.; Nahm, C.; Kim, J.; Moon, J.; Nam, S.; Jung, D.-R.; Park, B. The Effect of TiCl4-Treated TiO2 Compact Layer on the Performance of Dye-Sensitized Solar Cell. *Curr. Appl. Phys.* **2012**, *12* (3), 737–741.

(24) Snaith, H. J.; Moule, A. J.; Klein, C.; Meerholz, K.; Friend, R. H.; Grätzel, M. Efficiency Enhancements in Solid-State Hybrid Solar Cells via Reduced Charge Recombination and Increased Light Capture. *Nano Lett.* **2007**, *7* (11), 3372–3376.

(25) Garmaroudi, Z. A.; Abdi-Jalebi, M.; Mohammadi, M. R.; Friend, R. H. A Facile Low Temperature Route to Deposit a TiO 2 Scattering Layer for

Efficient Dye-Sensitized Solar Cells. *RSC Adv.* **2016**, *6* (75), 70895–70901.

(26) John, S.; Soukoulis, C.; Cohen, M. H.; Economou, E. N. Theory of Electron Band Tails and the Urbach Optical-Absorption Edge. *Phys. Rev. Lett.* **1986**, *57* (14), 1777–1780.

(27) Jackson, W. B.; Amer, N. M.; Boccara, a C.; Fournier, D. Photothermal Deflection Spectroscopy and Detection. *Appl. Opt.* **1981**, *20* (8), 1333–1344.

(28) Zhao, Y.; Nardes, A.; Zhu, K. Mesoporous Perovskite Solar Cells: Material Composition, Charge-Carrier Dynamics, and Device Characteristics. *Faraday Discuss.* **2014**, *176*, Ahead of Print.

(29) Bach, U.; Lupo, D.; Comte, P.; Moser, J. E.; Weissörtel, F.; Salbeck, J.; Spreitzer, H.; Grätzel, M. Solid-State Dye-Sensitized Mesoporous TiO2 Solar Cells with High Photon-to-Electron Conversion Efficiencies. *Nature* **1998**, *395* (6702), 583–585.

(30) Dar, M. I.; Abdi-Jalebi, M.; Arora, N.; Grätzel, M.; Nazeeruddin, M. K. Growth Engineering of CH 3 NH 3 PbI 3 Structures for High-Efficiency Solar Cells. *Adv. Energy Mater.* **2016**, *6* (2), 1501358.

(31) Ibrahim Dar, M.; Abdi-Jalebi, M.; Arora, N.; Moehl, T.; Grätzel, M.; Nazeeruddin, M. K. Understanding the Impact of Bromide on the Photovoltaic Performance of CH 3 NH 3 PbI 3 Solar Cells. *Adv. Mater.* **2015**, *27* (44), 7221–7228.

(32) Listorti, A.; Juarez-Perez, E. J.; Frontera, C.; Roiati, V.; Garcia-Andrade, L.; Colella, S.; Rizzo, A.; Ortiz, P.; Mora-Sero, I. Effect of Mesostructured Layer upon Crystalline Properties and Device Performance on Perovskite Solar Cells. *J. Phys. Chem. Lett.* **2015**, *6* (9), 1628–1637.

(33) Peng, W.; Anand, B.; Liu, L.; Sampat, S.; Bearden, B. E.; Malko, A.; Chabal, Y. J. Influence of Growth Temperature on Bulk and Surface Defects in Hybrid Lead Halide Perovskite Films. *Nanoscale* **2015**, 1627–1634.

(34) Senanayak, S. P.; Ashar, a Z.; Kanimozhi, C.; Patil, S.; Narayan, K. S. Room-Temperature Bandlike Transport and Hall Effect in a High-Mobility Ambipolar Polymer. *Phys. Rev. B* **2015**, *91* (11), 115302.

(35) Grancini, G.; Marras, S.; Prato, M.; Giannini, C.; Quarti, C.; De Angelis, F.; De Bastiani, M.; Eperon, G. E.; Snaith, H. J.; Manna, L.; et al. The Impact of the Crystallization Processes on the Structural and Optical Properties of Hybrid Perovskite Films for Photovoltaics. *J. Phys. Chem. Lett.* **2014**, *5* (21), 3836–3842.

(36) Graetzel, M.; Janssen, R. a J.; Mitzi, D. B.; Sargent, E. H. Materials Interface Engineering for Solution-Processed Photovoltaics. *Nature* **2012**, *488* (7411), 304–312.